


GEOLOGI FOR SAMFUNNET

GEOLOGY FOR SOCIETY



Report no.: 2012.017		ISSN 0800-3416	Grading: Confidential until March 2013
Title: Pockmarks, gas flares, tectonic features and processes leading to their formation, southwestern Barents Sea			
Authors: Shyam Chand, Terje Thorsnes, Leif Rise, Reidulv Bøe		Client: Lundin Norge AS	
County: Norway		Commune:	
Map-sheet name (M=1:250.000)		Map-sheet no. and -name (M=1:50.000)	
Deposit name and grid-reference:		Number of pages: 28	Price (NOK): 110,-
		Map enclosures: 0	
Fieldwork carried out:	Date of report: 23-2-2012	Project no.: 341300	Person responsible: 
Summary:			
<p>The project is aimed to achieve a better understanding of shallow geological/seabed conditions and processes to support technical and environmental aspects of exploration and production along the western margin of the Hammerfest Basin and Loppa High, and in the Tromsø Basin/Ingøydjupet area.</p> <p>The project has had the following subgoals:</p> <ul style="list-style-type: none"> • Detection of water column gas anomalies at selected pockmark locations • Identification of neotectonic features <p>The project has the following results:</p> <ul style="list-style-type: none"> • A total of 16 gas flares were identified using the water column data collected using the multibeam echosounder system during cruises in 2008 and 2009. The gas flares are observed to occur mainly outside the pockmark areas along regional faults where the seabed is incised by iceberg ploughmarks. No correlation is found between flare occurrence and tidal cycles but a full tidal cycle monitoring has not been carried out to substantiate it. • Pockmarks are interpreted to be formed after deglaciation due to melting of gas hydrates. They are probably not active at present. • Multiple fault/lineament locations were identified. They are observed to be of reverse faults with thrust part along the western side and deeper basin with larger sediment thickness along the eastern side. The faults are observed to be covered by undisturbed glaciomarine/marine sediments deposited after the last deglaciation, indicating little neotectonic activity. 			
Keywords: Marine Geology		Gas hydrate	Gas Flare
Pockmark		Seismic	Shallow Gas
Multibeam bathymetry		Water coloumn gas anomaly	Neotectonic faulting

CONTENTS

- 1. INTRODUCTION..... 7
- 2. STUDY AREA..... 8
- 3. MATERIALS AND METHODS 9
 - 3.1 Bathymetry/Backscatter..... 9
 - 3.2 TOPAS and HUGIN EdgeTech..... 10
 - 3.3 2D/3D Seismic..... 10
 - 3.4 Hydrate Stability Modelling 11
- 4. Pockmarks, prod marks, gas flares and neotectonics 12
 - 4.1 General morphology 12
 - 4.2 Pockmarks 12
 - 4.3 Gas flares 16
 - 4.4 Neotectonic structures 19
 - 4.5 Gas hydrates and fluid flow 21
- 5. CONCLUSIONS 26
- 6. REFERENCES 27

FIGURES

Figure 1. Bathymetry map of the SW Barents Sea showing the study area. Also shown are areas surveyed using EM710 multibeam echosounder and TOPAS (yellow polygons), 3D seismic (blue polygon), BSR occurrences (pink filled polygon), gas anomalies (purple polygons) (Andreassen and Hansen, 1995), faults at URU level (black lines), oil fields (red filled polygons) and Last Glacial Maximum (LGM) ice thickness contours (Siegert et al., 2001).

Figure 2. Regional bathymetry with area covered by detailed bathymetry from EM710 multibeam echosounder and 3D seismic (see fig 1 for locations). Also shown are locations of HUGIN EdgeTech 2200 data (black thick lines; thick black shaded areas in some locations are many closely spaced lines), gas flares (yellow triangles), gas anomalies (purple polygons), BSRs (pink polygons) (Andreassen and Hansen, 1995), hydrocarbon discoveries (red polygons), Late Weichselian Maximum- Stage II boundary (orange lines) (Winsborrow et al., 2010) and faults (black lines).

Figure 3. Multibeam a) bathymetry and b) backscatter from pockmark area (location given in Fig. 13). Notice the presence of pockmarks within depressions. The pockmarks have high backscatter at their centers indicating hard substrate or change in grain size.

Figure 4. TOPAS seismic across the pockmark area showing the various units. Only few pockmarks can be identified due to the large footprint of the hull mounted TOPAS system.

Figure 5. a) HUGIN EdgeTech 220 high resolution seismic section across a pockmark area (location shown on Fig. 13). b) Close up of one of the pockmarks. Notice the difference in structure between pockmarks and depressions. The pockmarks penetrate down to the marine/glaciomarine boundary (blue horizon), and some of them are identified to have highs within them. The depressions contain undisturbed marine/glaciomarine strata indicating that they formed prior to the deposition of these sediments.

Figure 6. Structural highs observed at the centre of pockmarks is unique to Barents Sea. a) EdgeTech 2200 seismic showing the general structure of centre high, b) seafloor structure of the centre high pockmark, c) backscatter associated with centre high pockmark. Notice that the high backscatter corresponds to the glaciomarine sediments at the base of the pockmark and also the centre high.

Figure 7. HUGIN TFish photo from the pockmark centre high showing blocks of consolidated sediments.

Figure 8. a) EdgeTech 2200 seismic data close to the boundary of the pockmark field. b) Bathymetry showing that the pockmarks become smaller. Location of a is highlighted in red line. The pockmarks become smaller where the soft sediment cover is thinner and that their presence is an indication of soft sediments on the seabed.

Figure 9. Gas flares from a) pockmark area and b) non pockmark area shown on shaded relief bathymetry. Notice that the flares originate at iceberg ploughmarks.

Figure 10. Time of multibeam data collection at gas flares plotted on tidal cycle curves from the Honningsvåg tidal station. One of the strongest flares observed was no. 98, occurring at high tide.

Figure 11. Multibeam bathymetry covering part of the fault area showing seafloor expressions of faults oriented in the NE-SW direction. The faults are observed to diverge into many branches towards the northeastern part of the study area.

Figure 12. Neotectonic faults mapped by EM710 and EdgeTech2200. a) EdgeTech2200 seismic profile across one of the faults where it changes orientation from NNE-SSW to NE-SW showing the occurrence of a pockmark in soft sediments above its termination. b) EdgeTech 2200 line across another part of the same fault showing undisturbed marine and galciomarine strata overlying it. The structural high indicates reverse faulting and/or deposition of material at the reverse faulted boundary. The eastern side of the structural high has more infill indicating deeper basin at that side. c) EdgeTech 2200 line across the fault where it is close to the seafloor giving high backscatter, d) Bathymetry showing the locations of several faults, e) Backscatter from location c indicating high backscatter along pockmarks and parts of some faults (black circles). Locations of a, b and c are indicated with red lines.

Figure 13. Structural map of the study area showing the thickness of structure II gas hydrate stability zone with 96% methane, 3% ethane and 1% propane. Also shown are areas of detailed multibeam bathymetry, faults (black lines), well locations, BSRs (pink polygons), gas anomalies (purple polygons) and gas flares (yellow triangles).

Figure 14. a) Present and b) LGM methane hydrate stability zone (MHSZ) thicknesses for southwestern Barents Sea estimated using bathymetry data, heat flow data (Bugge et al., 2002), bottom water temperature data (WOD, 2005) and ice thickness (Siegert et al., 2001). Notice the big change in methane hydrate stability since the LGM in our study area. Also shown are the gas flares (red triangles) and locations of MBB data (black polygons).

Figure 15. Details of the sedimentation history since the Last Glacial Maximum in Ingøydjupet from core JM05-08-GC (Aagard Sørensen et al., 2010). Notice the high sedimentation rates during the initial periods of deglaciation. During the last 9000 years

there was only 54 cm of sediment deposition in the deepest part of the Ingøydjupet indicating even less sedimentation in our study area.

Figure 16. a) Seismic section and b) fluid flow model towards gas flares showing subsurface geology and fluid flow. The fluids are transported along intra-Tertiary permeable formations and the base of the Tertiary while highly fractured Tertiary and Cretaceous sediments allow fluid flow through open faults. Notice the large amount of fracturing in the Plio-Pleistocene allowing fluid flow through glacial till. See Fig. 13 for location.

1. INTRODUCTION

The Barents Sea is an epicontinental sea bounded by a sheared and rifted Tertiary margin to the west (Eldholm et al., 1984). Mesozoic and early Cenozoic sedimentation took place in intracratonic basins. After the early Eocene opening of the Norwegian Sea, the Tertiary sediment transport bypassed these basins, and depocentres were established on the continental margin (Spencer et al., 1984). The Bear Island Trough was formed through extensive glacial erosion (Nøttvedt et al., 1988; Eidvin and Riis, 1989; Vorren et al., 1991; Riis and Fjeldskaar, 1992) and the bulk of the eroded sediments were deposited at the continental slope on the Bear Island Trough Mouth Fan (Vorren et al., 1991; Faleide et al., 1996). The morphology of the Barents Sea has been interpreted as a submerged, inherited fluvial landscape, formed in preglacial times and later modified by glacial erosion (Nansen, 1904; Lastochkin, 1977; Vorren et al., 1986, 1991; Laberg et al., 2011). Recent drilling and coring show that the main part of the erosion took place in the late Plio-Pleistocene (<2.7 Ma) and that the corresponding sediments have mainly a glacial affinity (Eidvin and Riis, 1989; Eidvin et al., 1993, 1998; Mørk and Duncan, 1993; Hald et al., 1990; Knies et al., 2009).

Estimates show that about 1000 m of sediments may have been removed by the erosion (Nøttvedt et al., 1988; Vorren et al., 1991; Riis and Fjeldskaar, 1992; Løseth et al., 1992; Nyland et al., 1992). The erosion produced a prominent erosion surface, the upper regional unconformity, URU (Solheim and Kristoffersen, 1984; Vorren et al., 1986). An upper glacial sediment sequence of varying thickness covers the URU (Solheim and Kristoffersen, 1984; Vorren et al., 1986). It reaches a maximum thickness of about 1000 m at the shelf edge, and has a secondary maximum on the inner shelf, adjacent to the Norwegian coast, where it fills a large glacial trough (Vorren et al., 1989, 1990). Associated with erosion, considerable late Cenozoic uplift took place, modeled by Riis and Fjeldskaar (1992) to 900-1400 m in the western Barents Sea. A major part of the fan is of late Pliocene and Pleistocene age (Eidvin and Riis, 1989; Eidvin et al., 1993), which implies very high erosion and sedimentation rates. High erosion rates for the mid-late Pleistocene were also inferred by Vorren et al. (1991), with 150 m regionally, and as much as 400 m locally, during the last 0.8 Ma, and by Sættem et al. (1992), who suggest erosion of 200-250 m or more for the last 0.44 Ma. Seismostratigraphic interpretations indicate that grounded glaciers may have reached the shelf break of the southern Barents Sea 5-10 times during the Pleistocene (Solheim and Kristoffersen, 1984; Vorren et al., 1988; Sættem et al., 1992).

This present study is focused on a small region along the south western Barents Sea and the western margin of the Hammerfest Basin, the Loppa High and the Tromsø Basin/Ingøydjupet area (Fig. 1). The project is aimed to achieve a better understanding of the shallow geological and seabed conditions and processes to support technical and environmental aspects of exploration within the study area. The project has the following subgoals:

- To detect pockmarks and seep-related features, including water column gas flares.
- To assess the occurrence and nature of faults and other neo-tectonic structures.

2. STUDY AREA

The study focuses on the western margin of the Hammerfest Basin/Loppa High and the Tromsø Basin/Ingøydjupet areas of the south western Barents Sea (Fig. 1). The study area is underlain by numerous regional faults oriented in the N-S direction and some of them branching out in the E-W direction (Fig. 2). The area is hydrocarbon prone with the Snøhvit field located south of the study area and the recent discovery of the Skrugard and the Havis fields (Fig. 2). The Skrugard discovery is located within the northernmost multibeam survey area. The northern part of the study area is also unique with the identification of a large number of subsurface gas anomalies and gas hydrate related bottom simulating reflectors (BSRs).

The region was under the influence of a thick ice sheet during the last Glacial Maximum (LGM), inferred to be 750-1000 m thick from modeling results (Siegert et al., 2001) (Fig. 1). The glaciers retreated from this region around 18000- 20000 cal years BP (14000-16000 C¹⁴ yrs) which resulted in huge release of ice load as well as deposition of glaciomarine and marine sediments. The exact timing of the retreat is still debated, but an early retreat was suggested by Aagard Sørensen et al. 2010 based on dating of a core from Ingøydjupet. The sedimentation rates during the glaciomarine period varied between 40 and 70 cm/kyr while it settled to a modest rate of 6 cm/kyr during the last 9000 cal years BP (Aagard Sørensen et al., 2010). The study area is also placed along the northernmost boundary of the Ingøydjupet depression where the basin shallows to a ridge like morainial high which represents the boundary of the stage II boundary of the late Weichselian glaciations (Winsborrow et al., 2010) (Fig. 2). The northern most part of the study area touches the southern boundary of the Bear Island Trough and hence is a location where many glacial advances coincide creating a chaotic pattern of depositional features (Winsborrow et al., 2010).

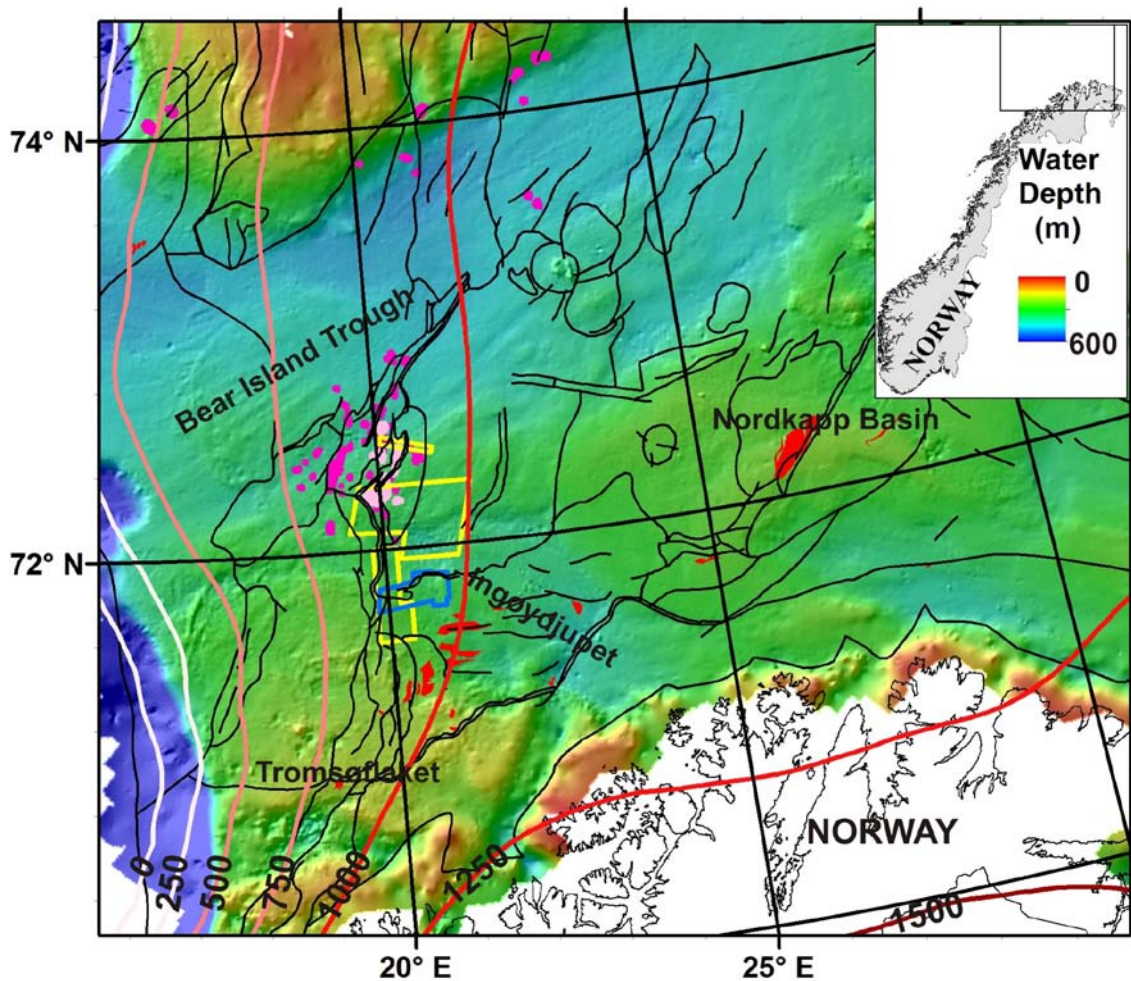


Figure 1. Bathymetry map of the SW Barents Sea showing the study area. Also shown are areas surveyed using EM710 multibeam echosounder and TOPAS (yellow polygons), 3D seismic (blue polygon), BSR occurrences (pink filled polygon), gas anomalies (purple polygons) (Andreassen and Hansen, 1995), faults at URU level (black lines), oil fields (red filled polygons) and Last Glacial Maximum (LGM) ice thickness contours (Siegert et al., 2001).

3. MATERIALS AND METHODS

3.1 Bathymetry/Backscatter

The multi beam bathymetry (MBB) data were collected by Forsvarets Forsknings Institutt (FFI) using EM710 echo sounder (Fig. 2). The main advantage of the multibeam echosounder system is that it can record the water column data also. The operating frequency (70-100 kHz) is also advantageous for the intermediate water depths, between 200 m and 1000 m, where other systems usually need a change in frequency. The operating frequency of 70-100 kHz and water depths of ca. 350 m give a Fresnel zone diameter (foot print) of around 4 m thus mapping 13 m² by each beam. As a general rule, features smaller than the size of one fourth

the wavelength cannot be resolved (Sheriff, 1980). Hence, features larger than 1 meter in diameter can be theoretically detected using the system. The water column data recorded by the system can be used for detection of active gas seeps and also detection of fauna. Presences of fish schools can be easily identified and is hence useful to estimate the energy loss in the water column during detailed back scatter processing. The FlederMaus (FM) Midwater package was used to analyse the water column data for detecting and analysing gas anomalies. The MBB data can also be used to derive the seafloor reflection (i.e., backscatter) properties which will indirectly give an indication of sediment type/grain size and/or hardness of the sea bottom. The FM Geocoder package was used to process the MBB data for backscatter.

3.2 TOPAS and HUGIN EdgeTech

The TOPAS parametric subbottom profiler was used to acoustically map parts of the study area to resolve sediment stratigraphy in the uppermost part of the seabed (Fig. 1). Layering can be clearly interpreted if the source signal can penetrate the seafloor sediments thus giving a detailed stratigraphy going up to few tens of thousands of years. An EdgeTech 2200 high resolution full spectrum chirp sub-bottom profiler (SBP) mounted on FFI's AUV HUGIN HUS, operated from HU Sverdrup II was used to map interesting areas of the immediate subsurface in very high resolution (Fig. 2). The HUGIN HUS was flown ~10 m above the seafloor at a constant speed giving 50 cm horizontal resolution and a vertical resolution of less than 100 microseconds (~10 cm) with the SBP system. The HUGIN EdgeTech data are available to the user as Segy files without correction for water depth. The data were corrected for water depth using the Vista Seismic Processing package and also using in house software the geographic coordinates were converted to UTM coordinates with centimetre accuracy and uploaded to the header.

3.3 2D/3D Seismic

The conventional 2D seismic covering the study area and the nearby region gives a regional perspective of the study area in relation to the surrounding geology. The occurrences of stratigraphic discontinuities and sedimentary strata in relation to structural features can be clearly delineated using these regional 2D seismic lines. The 3D seismic data, LHS08M01 (Fig. 1), from the study area gives a detailed picture of the subsurface anomalies observed at the shallow subsurface and can be used as guidance for interpreting anomalies. The interpretations carried out during the first phase of this project (Chand et al., 2009; NGU Report 2009.041) was available for analysing results obtained in the present phase of the project.

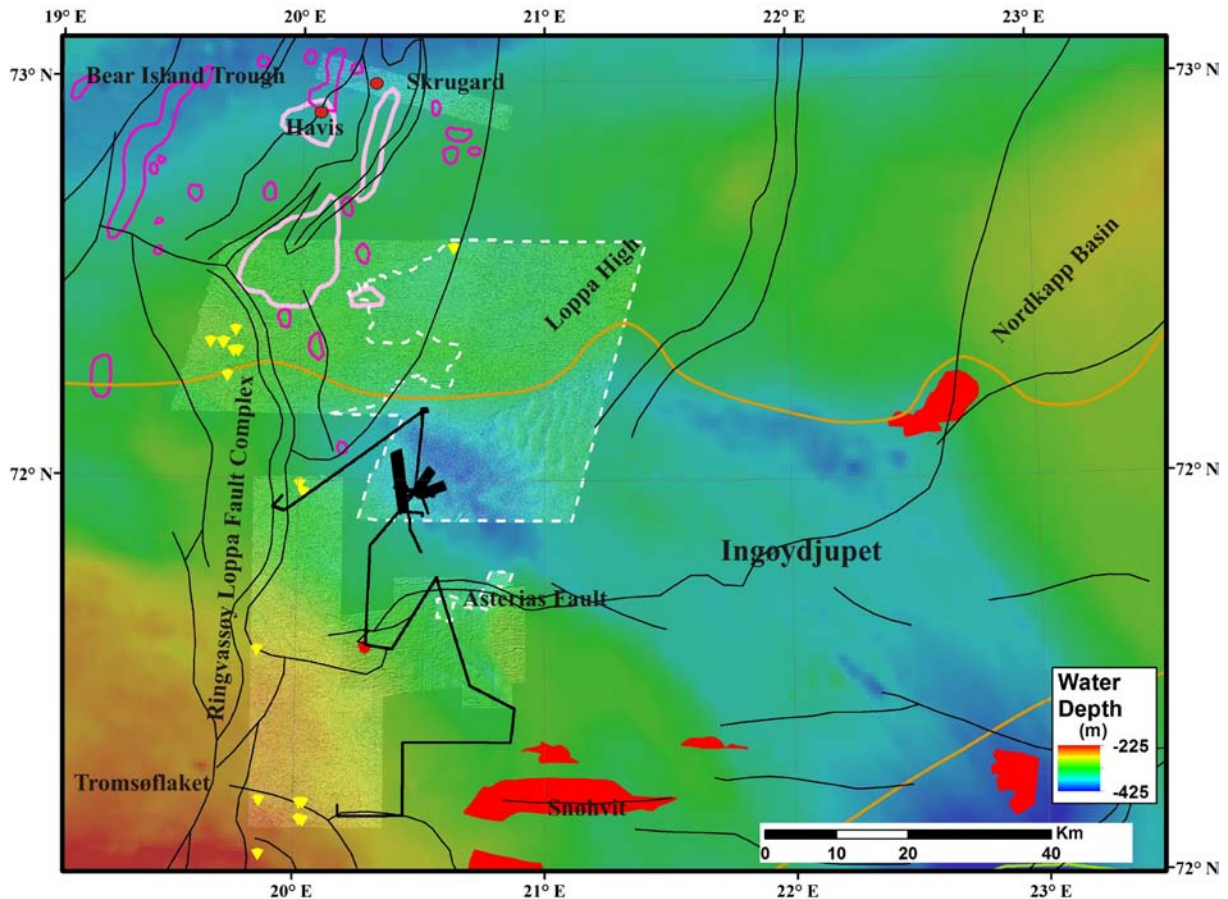


Figure 2. Regional bathymetry with area covered by detailed bathymetry from EM710 multibeam echosounder and 3D seismic (see fig 1 for locations). Also shown are locations of HUGIN EdgeTech 2200 data (black thick lines; thick black shaded areas in some locations are many closely spaced lines), gas flares (yellow triangles), gas anomalies (purple polygons), BSRs (pink polygons) (Andreassen and Hansen, 1995), hydrocarbon discoveries (red polygons), Late Weichselian Maximum- Stage II boundary (orange lines) (Winsborrow et al., 2010) and faults (black lines).

3.4 Hydrate Stability Modelling

Present and Last Glacial Maximum (LGM) thickness of the methane hydrate stability zone (MHSZ) for the Barents Sea was modelled using a modified version of the gas hydrate stability modelling program CSMHYD (Sloan, 1990; Chand et al., 2008). A smooth bathymetry model available for the whole southwestern Barents Sea (Fig. 1), available heat flow values (Bugge et al., 2002) and measured bottom water temperature values (WOD, 2005) were used to predict the present MHSZ thickness. MHSZ thickness during the LGM was modelled using ice thickness models (Fig. 1) proposed for this area (Siegert et al., 2001) and ice bottom (seabed) temperature of 0°C. The gas hydrate stability zone thickness model for 96% methane, 3% ethane and 1% propane were also calculated using the same parameters (Fig. 11). The hydrate stability field along the southern part of the study area could be deeper;

based on the well reports from nearby wells, that high amount of CO₂ (6%) and H₂S (3 ppm) is present (NPD, 2005; for e.g., NPD well report 7021/4-1).

4. Pockmarks, prod marks, gas flares and neotectonics

4.1 General morphology

The multibeam bathymetry collected during this project is located along the northern part of Tromsøflaket and the northernmost part of Ingøydjupet. Water depths range from 235 m to 425 m, with largest depths in northernmost part of Ingøydjupet (Fig. 2). The bathymetry shows some very interesting features indicating moraine ridges like along the eastern part of the multibeam area in Ingøydjupet and at the southernmost extent of the stage II of the Weichselian glaciations (Fig. 2). Iceberg ploughmarks criss-cross the whole area except where covered by a thicker unit of soft sediments. The seabed has varying hardness indicated by the variation in backscatter. The deeper areas have comparatively low reflectance, caused by a soft sediment cover. Small pockmarks are observed at the northern part of Ingøydjupet while larger depressions (prod marks probably formed by icebergs) are observed scattered all along the study area.

4.2 Pockmarks

Large density of pockmarks occurs almost exclusively in the deepest part of the study area. These pockmarks are generally circular with less than 50 m in diameter and up to 2 m deep, with an average density of c. 150 pockmarks per square kilometer (Fig. 3a). The pockmarks are either randomly distributed, or occur in arrays along iceberg plough marks. The pockmarks become smaller in diameter and depth close to the boundaries of Ingøydjupet and also on top of faults where the soft sediment thickness is thin. Most pockmarks are observed to have higher backscatter than the surrounding sediments (Fig. 3b) indicating coarse grain size/hard substrate.

Large, irregular depressions with diameters up to 300 m, depths up to 25 m, and with wall slopes up to 30° are observed scattered around the study area (Fig. 3a). They have irregular rims, and iceberg ploughmarks occasionally start or end in these depressions, while others have no obvious relation to plough marks. In many cases pockmarks occurs within these large depressions indicating that they formed prior to the pockmarks. The backscatter shows that the depressions do not exhibit specific anomalies compared to the surrounding seabed indicating that these features have similar type of sediments to that present outside (Fig. 3b).

The TOPAS data give high resolution images of the subsurface (Fig. 4). The inferred boundary between glaciomarine and marine sediments and the interface with the underlying till deposits can be mapped using the TOPAS data. The TOPAS data cannot however resolve small pockmarks or the structure of pockmarks due to the large foot print and low resolution compared to the HUGIN data.

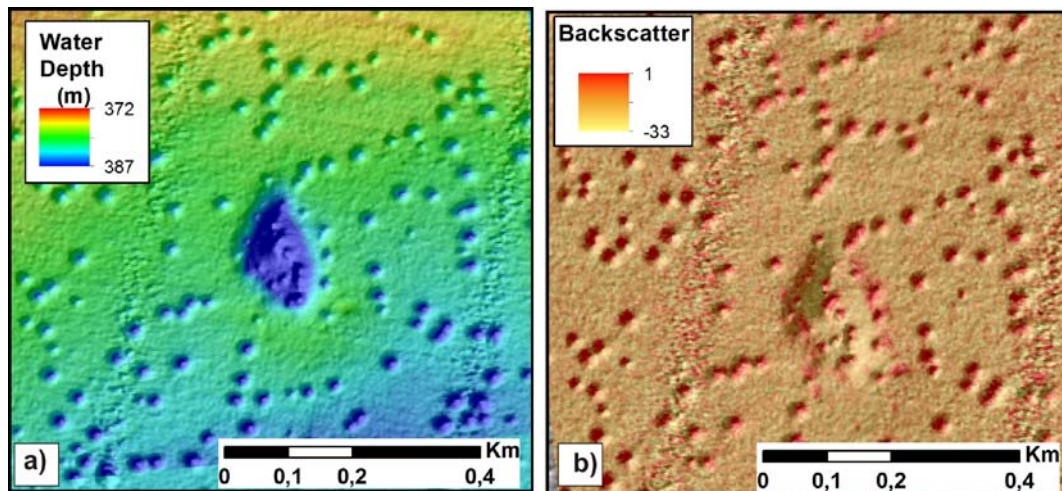


Figure 3. Multibeam a) bathymetry and b) backscatter from pockmark area (location given in Fig. 13). Notice the presence of pockmarks within depressions. The pockmarks have high backscatter at their centers indicating hard substrate or change in grain size.

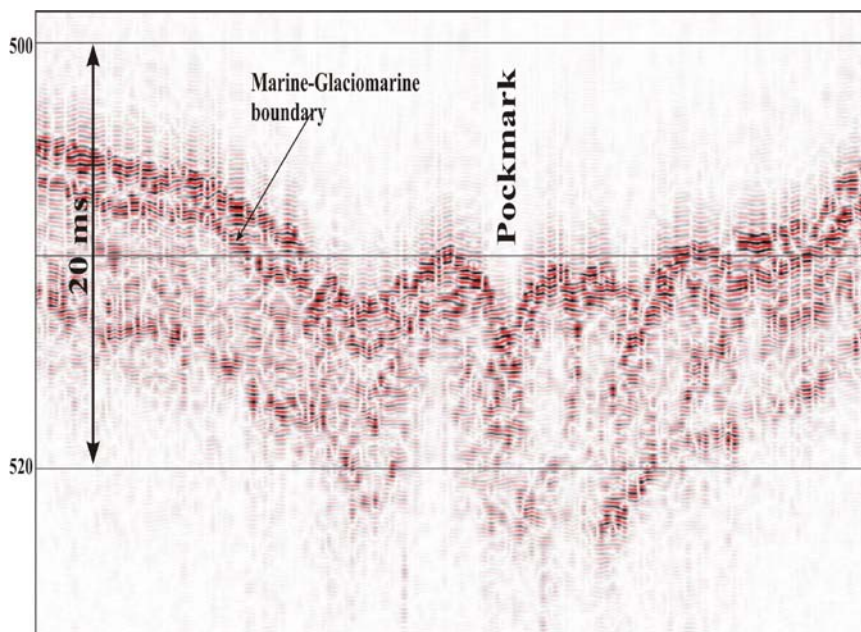


Figure 4. TOPAS seismic across the pockmark area showing the various units. Only few pockmarks can be identified due to the large footprint of the hull mounted TOPAS system.

The very high resolution Edgetech 2200 SBP data from HUGIN give detailed images of pockmarks and subsurface stratigraphy (Fig. 5a). Pockmarks are observed to cut across glaciomarine reflectors a few milliseconds below the seafloor indicating that they formed

after the end of glaciomarine sedimentation (Fig. 5a). Glaciomarine deposits underlying the pockmarks appear to be little influenced by their formation, indicating that they generally formed by slow seeping of fluids (Fig. 5a). The pockmarks have only a thin fill of marine sediments implying that the fluid flow was active until the major sedimentation cycle was over after deglaciation (Figs. 5a & 5b). The glaciomarine sediments appear as stratified layers indicating that clear boundaries exist within these sediments (Figs. 5a & 5b). These high reflective layers could be the reason for the high backscatter observed at the centre of pockmarks.

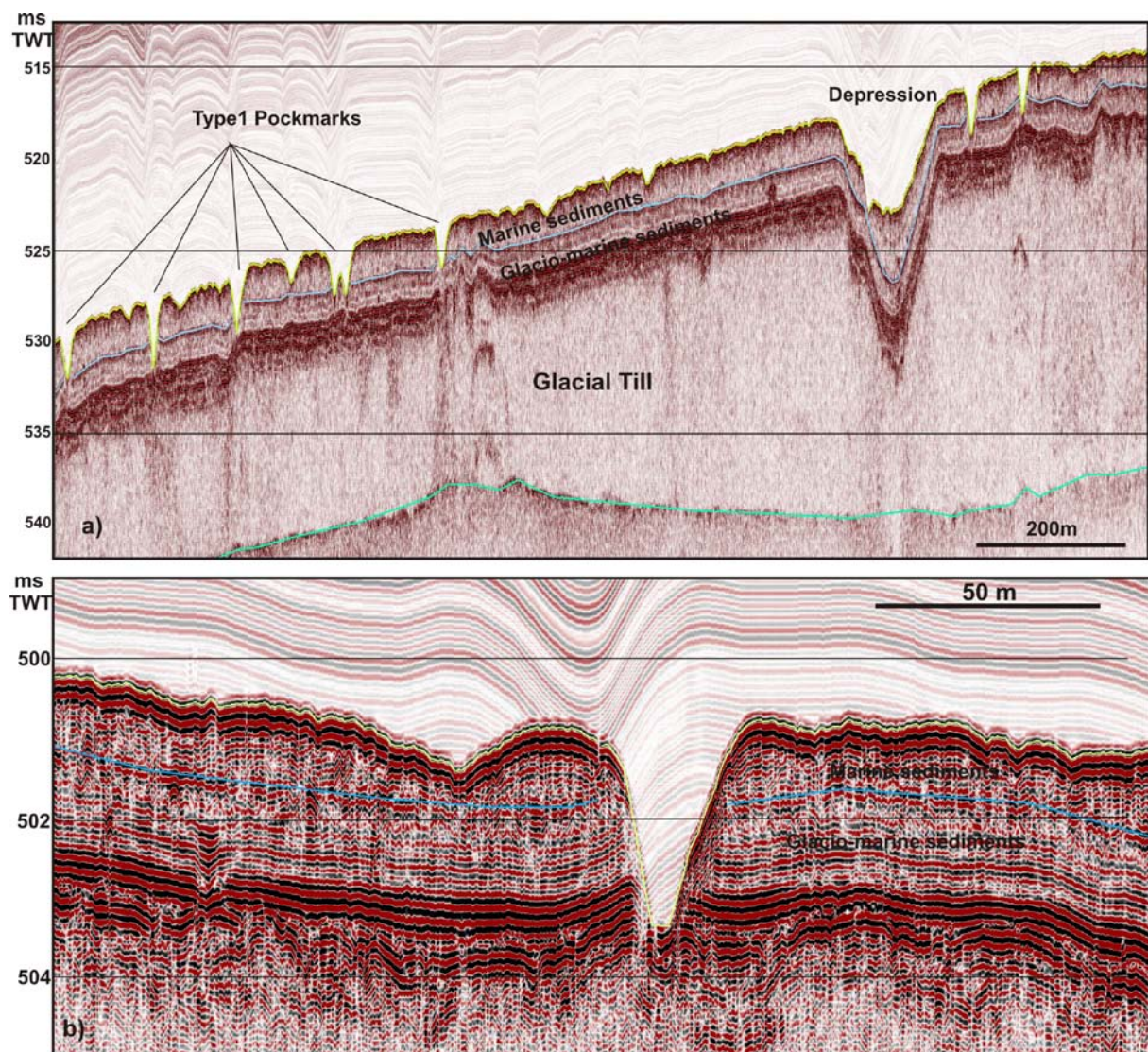


Figure 5. a) HUGIN EdgeTech 220 high resolution seismic section across a pockmark area (location shown on Fig. 13). b) Close up of one of the pockmarks. Notice the difference in structure between pockmarks and depressions. The pockmarks penetrate down to the marine/glaciomarine boundary (blue horizon), and some of them are identified to have highs within them. The depressions contain undisturbed marine/glaciomarine strata indicating that they formed prior to the deposition of these sediments.

Depressions are observed to have infill of both marine and glaciomarine sediments indicating that they formed before or during deposition of the glaciomarine unit (Fig. 5a). Till underlying the depressions appears to be disturbed indicating that they could be formed by plunging of icebergs on to the seafloor or from explosive expulsion of fluids (Fig. 5a). The relatively uniform backscatter observed in depressions compared to outside can be hence explained by this continuous sediment sequence. Similar large depressions containing gas hydrates are observed north of the Bear Island Trough which are interpreted to have formed through explosive release of fluids (Solheim and Elverhøi, 1985; Long et al., 1998).

Pockmarks sometimes exhibit structural highs along their centres (Fig. 6). The backscatter data indicates that they have high backscatter associated with it. The EdgeTech 2200 seismic shows that these highs contain high reflective material similar to those of early glaciomarine sedimentation (Fig. 6). TFish photos collected along the centre high indicate consolidated sedimentary slab like material (Fig. 7), similar to those observed in the pockmark field north of Bear Island Trough (Long et al., 1998). Pockmarks are absent over half of the multibeam surveyed area. The Edgetech 2200 data indicates that the absence of pockmarks is related to absence/very thin deposits of marine sediments (Fig. 8).

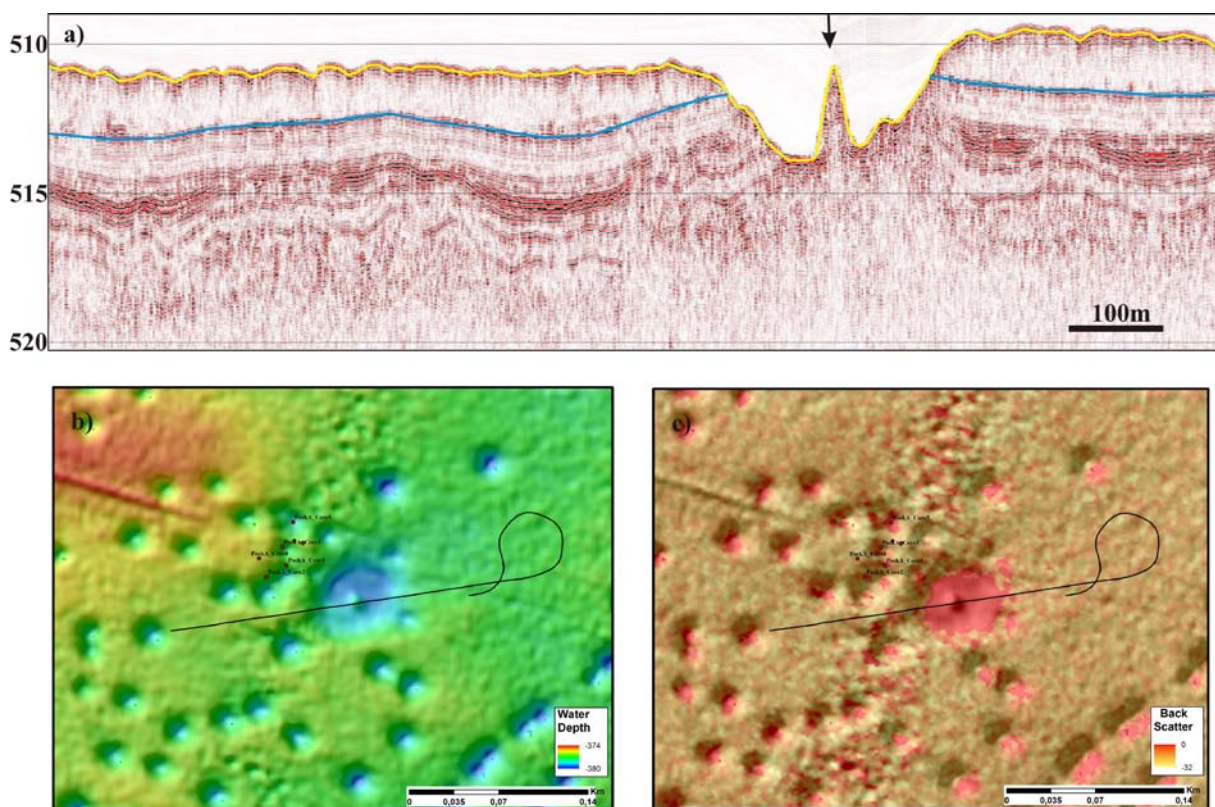


Figure 6. Structural highs observed at the centre of pockmarks is unique to Barents Sea. a) EdgeTech 2200 seismic showing the general structure of centre high, b) seafloor structure of the centre high pockmark, c) backscatter associated with centre high pockmark. Notice that the high backscatter corresponds to the glaciomarine sediments at the base of the pockmark and also the centre high.

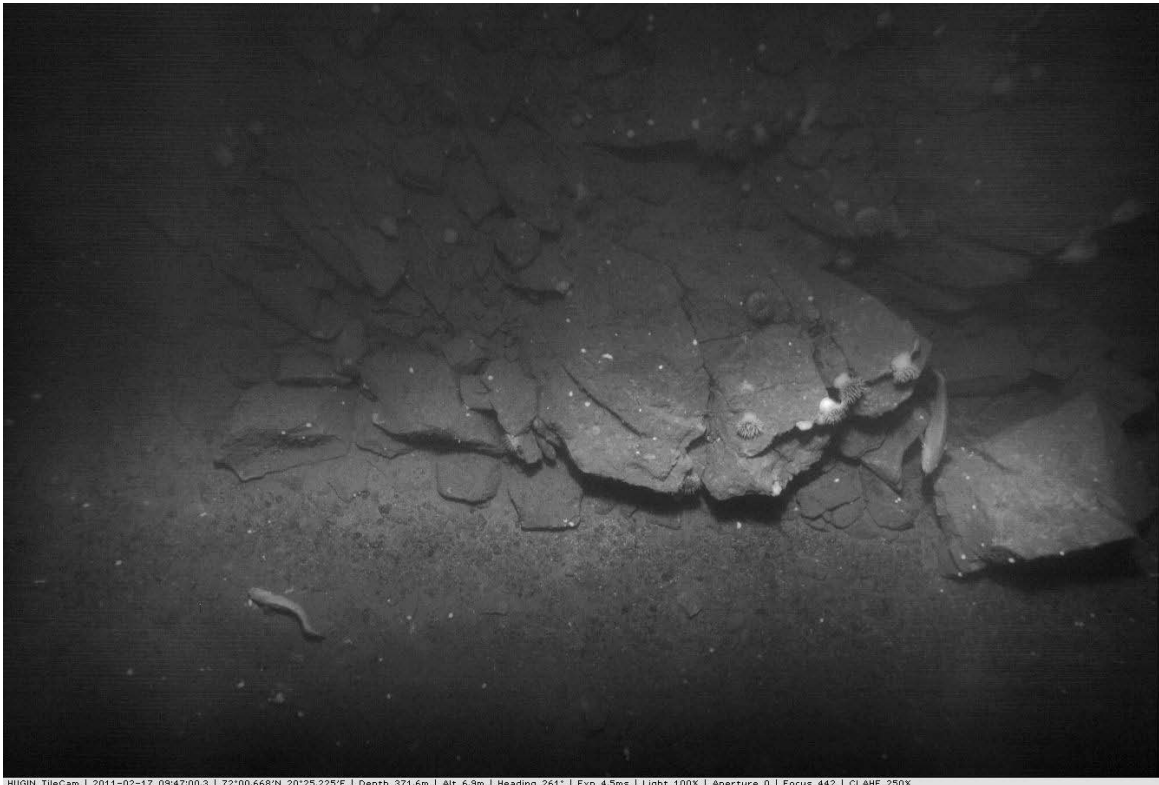


Figure 7. HUGIN TFish photo from the pockmark centre high showing blocks of consolidated sediments.

4.3 Gas flares

The use of water column data brought a new dimension to the study of subsurface fluid flow through the detection of acoustic gas flares. Water column data analyses using the FlederMaus Midwater package indicates 16 acoustic gas flares in the area covered by the multibeam data (Figs. 2, 9a & b). The majority of flares occur outside the pockmark areas. The flares are as high 200 m (Fig. 9b). One of the flares is located in the pockmark area close to a branch of the Ringvassøy Loppa Fault Complex (RLFC) (Fig. 2 & 9b). The flares are mainly located close to iceberg ploughmarks indicating that deep scouring by icebergs created deep incisions on the seafloor and fractures in the subsurface where gas can leak. The strength and height it reaches in the water column vary from one flare to other. Most of the flares fall into two clusters. The flares fall in the vicinity of regional faults which comprises of many faults reaching upto the base Plio-Pleistocene (URU) boundary indicating that the origin of fluids are deep (Fig. 2).

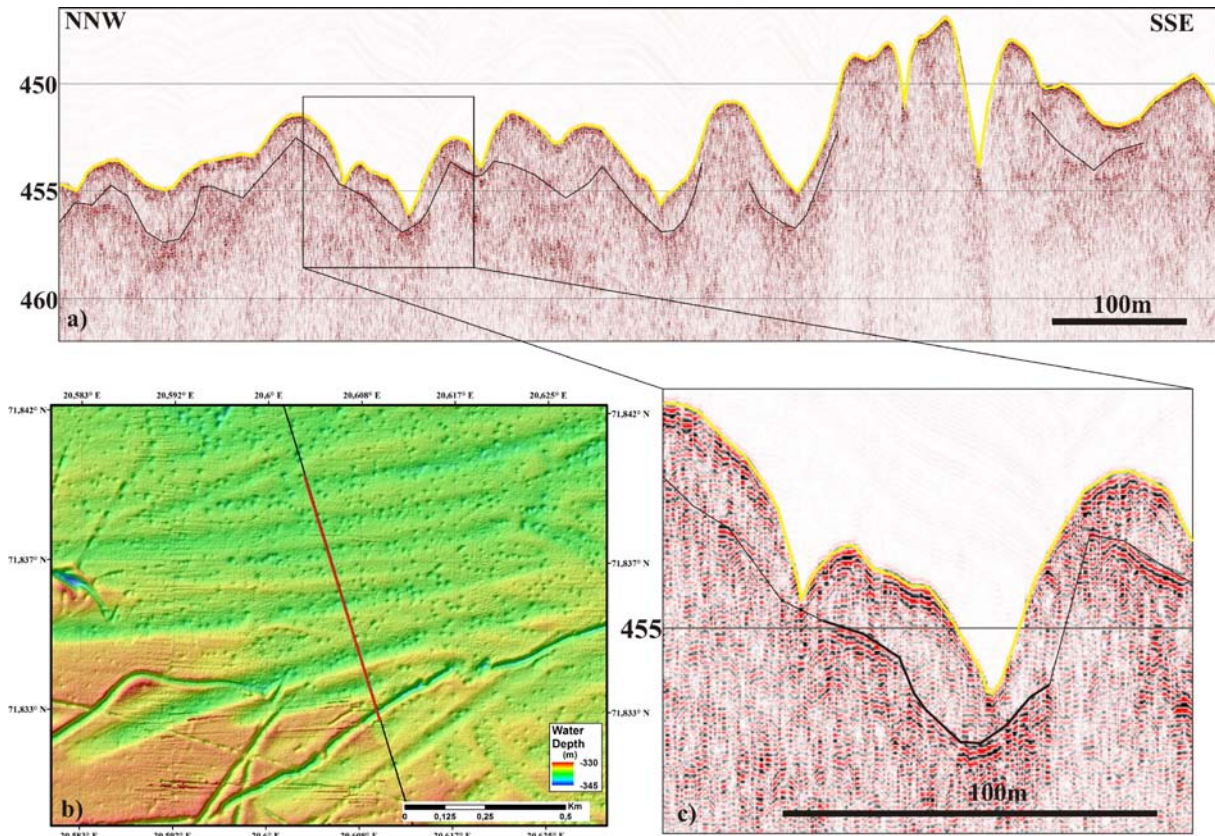


Figure 8. a) EdgeTech 2200 seismic data close to the boundary of the pockmark field. b) Bathymetry showing that the pockmarks become smaller. Location of a is highlighted in red line. The pockmarks become smaller where the soft sediment cover is thinner and that their presence is an indication of soft sediments on the seabed.

Analysis of flares in comparison to tidal data from the near shore tide station at Honningsvåg indicates no correlation to tidal cycles (Fig. 10). However, the analysis was not done on continuous tidal cycle and hence it could be that the data were collected when the flares were less active. Similar correlation to tidal data at the Hola site off Vesterålen indicated direct correlation to tidal cycles, where the flares occur or become more active just after the highest point of the tidal cycle. It indicates that there could be more flares existing in the study area and also some of the flares may be stronger than observed at present due to the timing of date collection in relation to tidal cycle.

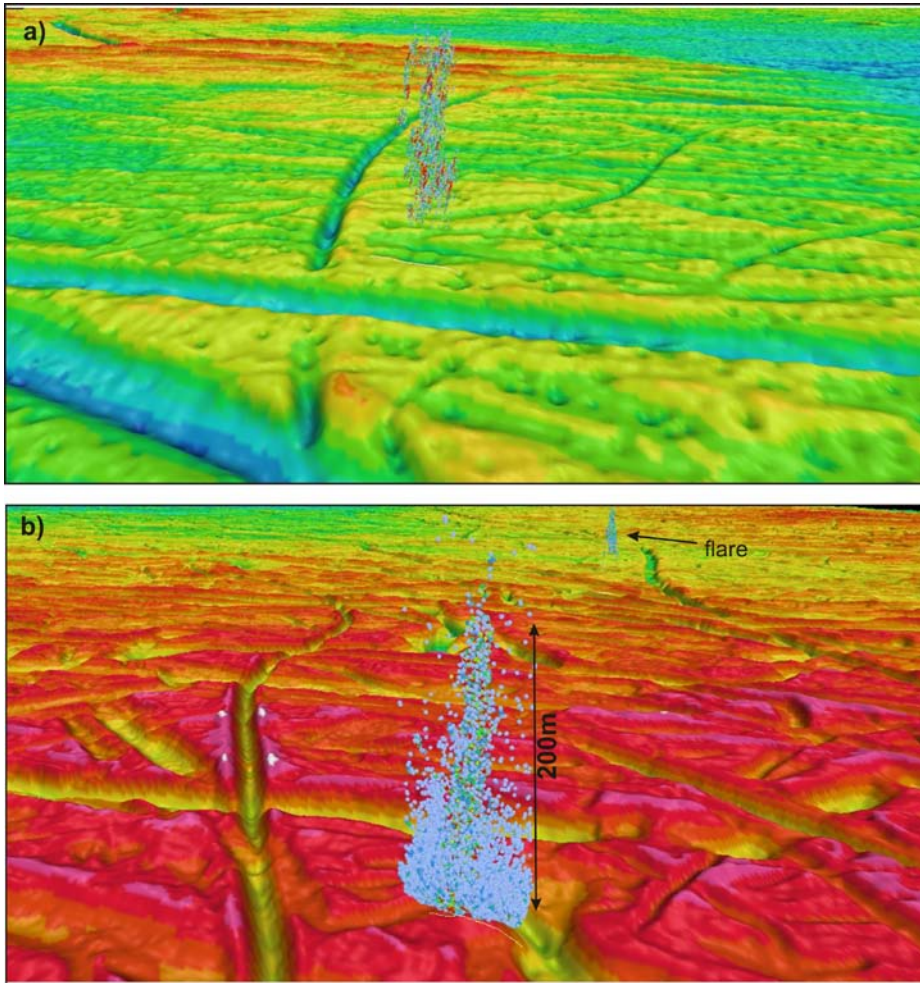


Figure 9. Gas flares from a) pockmark area and b) non pockmark area shown on shaded relief bathymetry. Notice that the flares originate at iceberg ploughmarks.

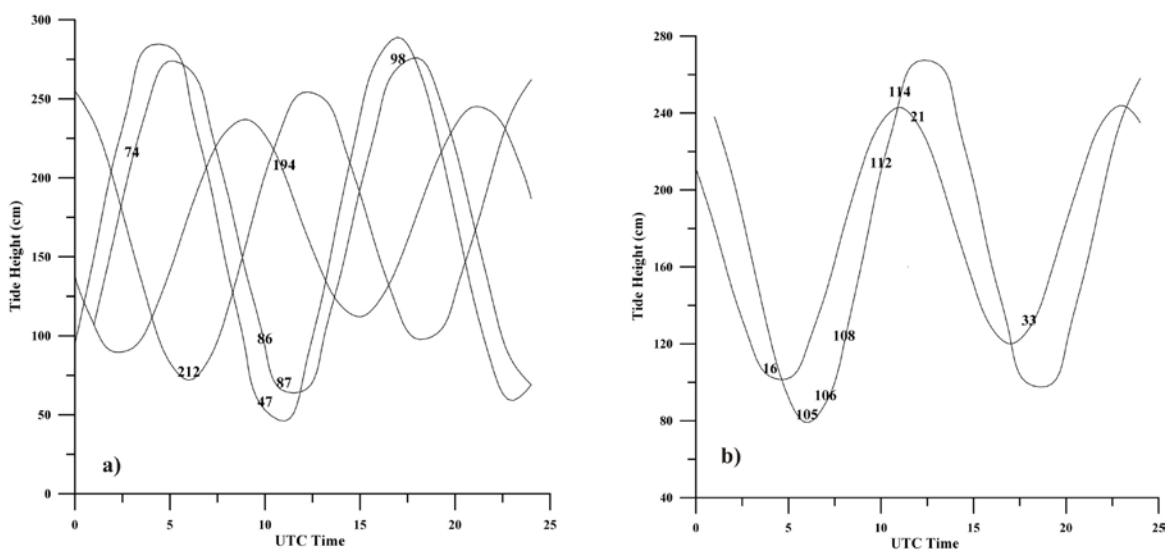


Figure 10. Time of multibeam data collection at gas flares plotted on tidal cycle curves from the Honningsvåg tidal station. One of the strongest flares observed was no. 98, occurring at high tide.

4.4 Neotectonic structures

Multibeam bathymetry and HUGIN Edgetech 220 data were analysed to map surface expressions of possible neotectonic features and their relation to subsurface structures. A large number of fault like features, oriented in NE-SW direction, were observed as elevated lineaments along the eastern part of the study area. The fault like features are partly covered by sediments in deeper areas while they are well exposed along the morainal ridges (Fig. 11). Small pockmarks occur on top of these highs at some locations indicating that they are partly covered by marine sediments and that the thickness of soft sediments is sufficient for pockmark formation (Fig. 12). Since the marine sediments appear to be undisturbed and the pockmarks are small we assume that the fault like features were formed prior to the deposition of the marine sediments and hence are not active at present (Fig. 12). It can be also observed that the features appear as structural highs on seismic data (Figs. 12 a, b & c) indicating that they could have been formed through reverse faulting and/or are edge morainal features created along these palaeo fault boundaries. The sediment thickness along the eastern side of the fault is observed to be thicker and the stratigraphic boundaries deeper indicating upward movement along the western side of the reverse fault. The features has to be analysed further using deeper airgun seismic data. High backscatter observed along some parts of faults are observed to be due to the exposure of them at the seafloor (Figs. 12 c & e).

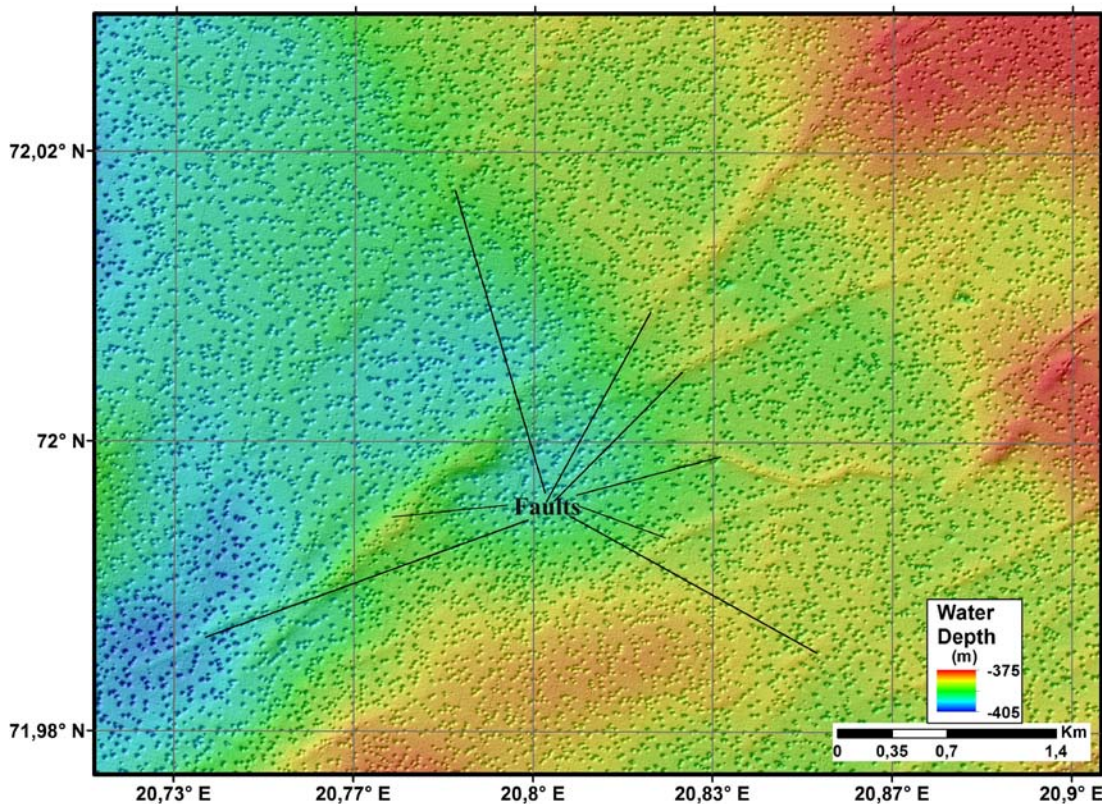


Figure 11. Multibeam bathymetry covering part of the fault area showing seafloor expressions of faults oriented in the NE-SW direction. The faults are observed to diverge into many branches towards the northeastern part of the study area.

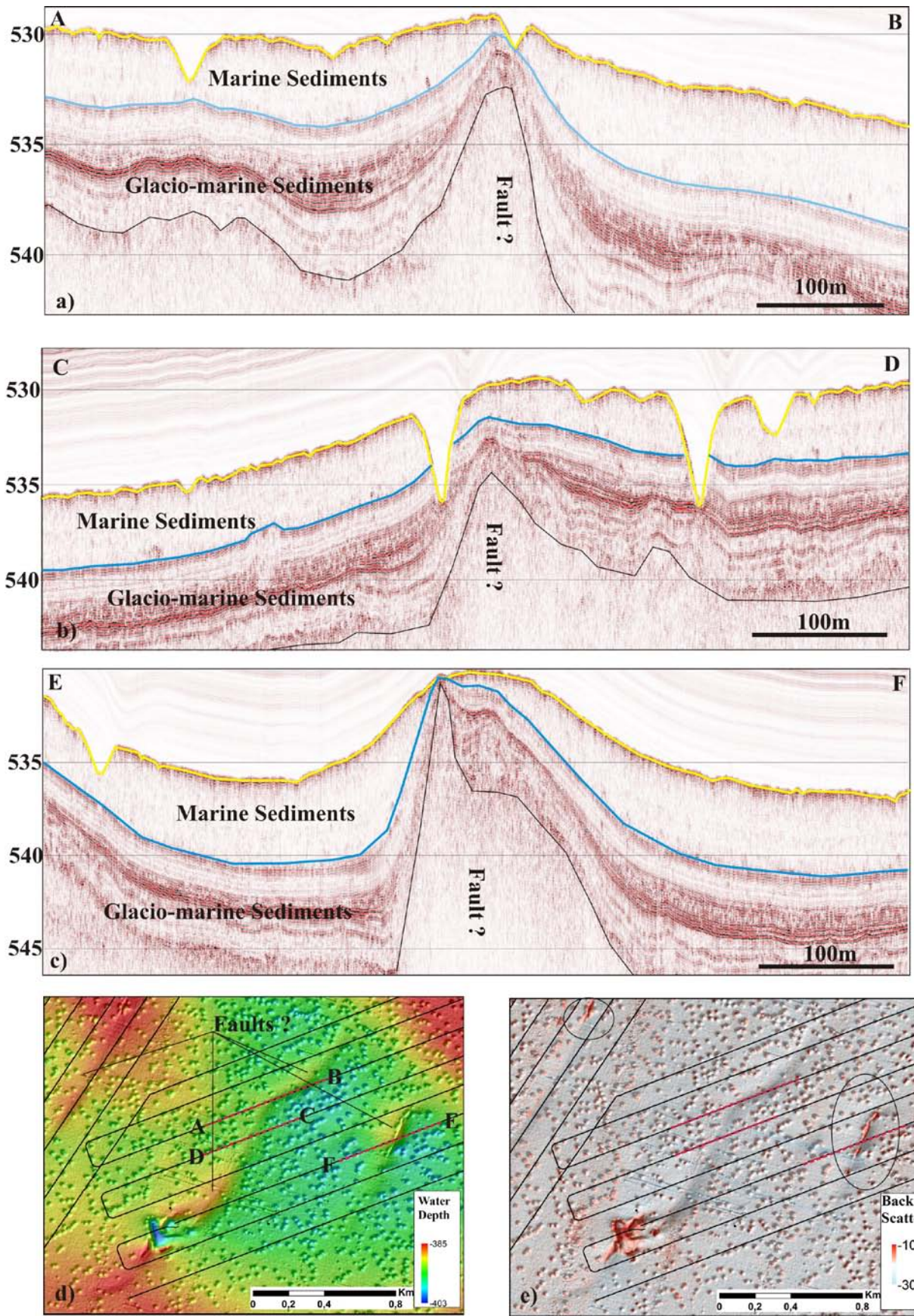


Figure 12. Neotectonic faults mapped by EM710 and EdgeTech2200. a) EdgeTech2200 seismic profile across one of the faults where it changes orientation from NNE-SSW to NE-

SW showing the occurrence of a pockmark in soft sediments above its termination. b) EdgeTech 2200 line across another part of the same fault showing undisturbed marine and galciomarine strata overlying it. The structural high indicates reverse faulting and/or deposition of material at the reverse faulted boundary. Tthe eastern side of the structural high has more infill indicating deeper basin at that side. c) EdgeTech 2200 line across the fault where it is close to the seafloor giving high backscatter, d) Bathymetry showing the locations of several faults, e) Backscatter from location c indicating high backscatter along pockmarks and parts of some faults (black circles) . Locations of a, b and c are indicated with red lines.

4.5 Gas hydrates and fluid flow

Gas hydrates in offshore areas are often associated with a bottom simulating reflector (BSR) . A BSR is a seismic reflector which sub-parallel the seafloor reflection and is opposite in polarity (Shipley et al., 1979). The BSR indicates an acoustic impedance change across a high velocity layer of gas hydrate containing sediments overlying a gas filled layer (Stoll and Bryan, 1979). The BSR is paralleling the seafloor since the thickness of the gas hydrate stability zone (GHSZ) is primarily decided by the hydrostatic pressure induced by the water column thickness (Sloan, 1990).

Nature and properties of BSRs and their occurrence vary depending on the sedimentary environment and fluid flow (Chand and Minshull, 2003). It is observed in many parts of the world that the BSR depths are altered by the presence of one or more of the gas hydrate inhibitors (NaCl, N₂, warm fluids, isostatic uplift, sliding, deglaciation) or facilitators (CO₂, H₂S, higher order hydrocarbon gases, increase in sea level, subsidence). Hydrates formed from pure methane assume molecular structure I while in the presence of higher order hydrocarbon gases it takes structure II. Structure I and II gas hydrates have different stability conditions and physical properties. Hence, it is complicated to interpret the presence of gas hydrates in areas with mixed gas origin causing disturbed BSRs, or in regions outside the methane hydrate stability field where all the gas hydrate is formed as structure II. The BSR or gas hydrate stability zone is shifted due to changes in sea level, variations in ice thickness or due to influx of warm or salty fluids from below, altering gas hydrate stability conditions. The present regional gas hydrate stability estimated for structure II hydrates containing higher order hydrocarbon gases for the Barents Sea indicates a ~250 m deep base of the GHSZ covering the study area while the structure I MHSZ is zero using a gas composition consisting of 96% methane, 3% ethane and 1% propane (Chand et al., 2008) (Fig. 13). The estimated two way time (TWT) milliseconds (ms) thickness of the GHSZ is around 220-270 ms assuming 1990 m/s velocity for the sediments (observed at well 7220/2-1).

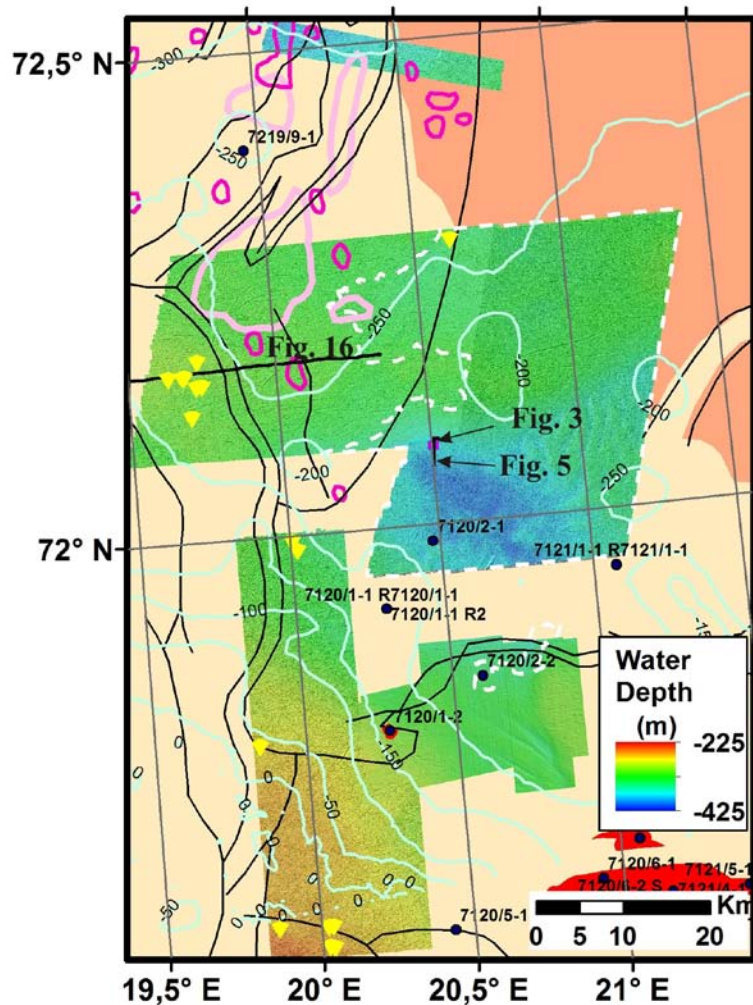


Figure 13. Structural map of the study area showing the thickness of structure II gas hydrate stability zone with 96% methane, 3% ethane and 1% propane. Also shown are areas of detailed multibeam bathymetry, faults (black lines), well locations, BSRs (pink polygons), gas anomalies (purple polygons) and gas flares (yellow triangles).

High amounts of CO₂ (up to 6%) and H₂S (3 ppm) are reported from the Snøhvit area in many wells, indicating that CO₂ and H₂S may be of importance while modelling the gas hydrate stability for this region (NPD, 2005; for eg., NPD well report 7021/4-1). The regional MHSZ estimated for the Barents Sea indicates a base 0 to 250 m deep the seafloor depending on the present day bathymetry and bottom water temperature (Fig. 14a). During the last glacial maximum (LGM), about 20 000 ¹⁴C years ago, a more than 1200 m thick ice cap covered the SW Barents Sea (Siegert et al., 2001). This made the whole SW Barents Sea stable for methane hydrate with MHSZ depths up to 600 m below the present seafloor (Fig. 14b). The difference between the present MHSZ and that during LGM indicates a change of thickness by up to 600 m. The MHSZ within the Bear Island Trough (BIT) thinned to less than 250 m while most other parts of the southwestern Barents Sea including our study area lie outside the MHSZ. The major change occurred outside the BIT, which made this region prone to release of methane accumulated during the last glaciation as methane hydrates. Our study area experienced a change in MHSZ of 500 m to zero m during this change in ice

thickness. The study area is also located close to the boundary of the Loppa High where the prograding wedges of glacial debris pinch out causing upward focusing of fluids towards the eastern flank of the Loppa High. The study area is also transected by a large number of regional faults, including the Ringvassøy Loppa Fault Complex and the Asterias fault, facilitating upward fluid flow.

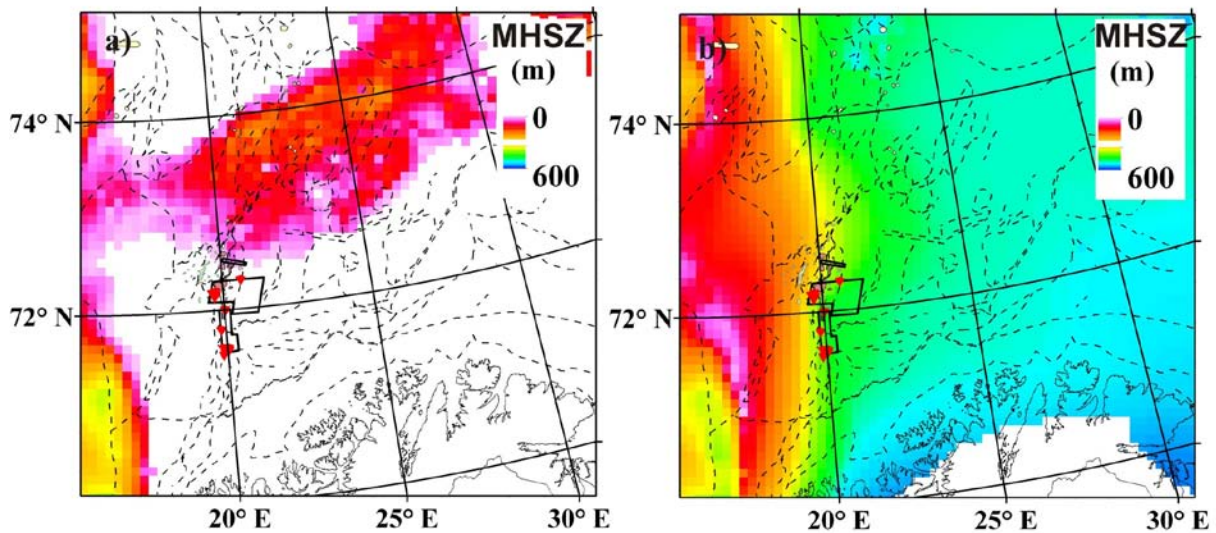


Figure 14. a) Present and b) LGM methane hydrate stability zone (MHSZ) thicknesses for southwestern Barents Sea estimated using bathymetry data, heat flow data (Bugge et al., 2002), bottom water temperature data (WOD, 2005) and ice thickness (Siegert et al., 2001). Notice the big change in methane hydrate stability since the LGM in our study area. Also shown are the gas flares (red triangles) and locations of MBB data (black polygons).

The fluid flow model for the study area is hence complex due to the two stage process which governed the accumulation and release of fluids including gas. In the first case, fluids and methane accumulated as methane hydrates under the thick glaciers during the LGM and were released during the deglaciation which created the pockmarks. This can be confirmed since the pockmarks appear to have formed after the rapid deposition of glaciomarine sediments and earliest phase of marine sedimentations. The stratigraphic layers in the glaciomarine unit are cut by pockmarks indicating that the sediments were removed once the gas hydrate started melting after the glaciers retreated from this region. The process has a time delay and probably stopped after some time indicated by the presence of few centimeters of marine sediments in pockmarks (UiO and GFZ results). The sedimentation rate in the deepest part of the Ingøydjupet is reported to be 6 cm/kyr during the last 9000 cal years. This indicates deposition of 54 cm of sediments at the location of JM05-085_GC. Our study area is located along the shallower part of the Ingøydjupet indicating that the sedimentation rate could have been even lower. This can be noticed by comparing the EdgeTech2200 seismic with the JM05-08-GC core. In JM05-08-GC a total of 2.5 metres of marine sediments is reported (Fig. 15) while the Edgetech2200 from the study area shows about 2 ms TWT of marine sediments (Figs. 5 & 12) which will correspond to 1.6 m (1600 m/s) marine sediments in the study area.

The stratified glaciomarine package is also present in the study area similar to that observed at the JM05-08-GC core location. Thus the formation of pockmarks can be related to the deglaciation after LGM.

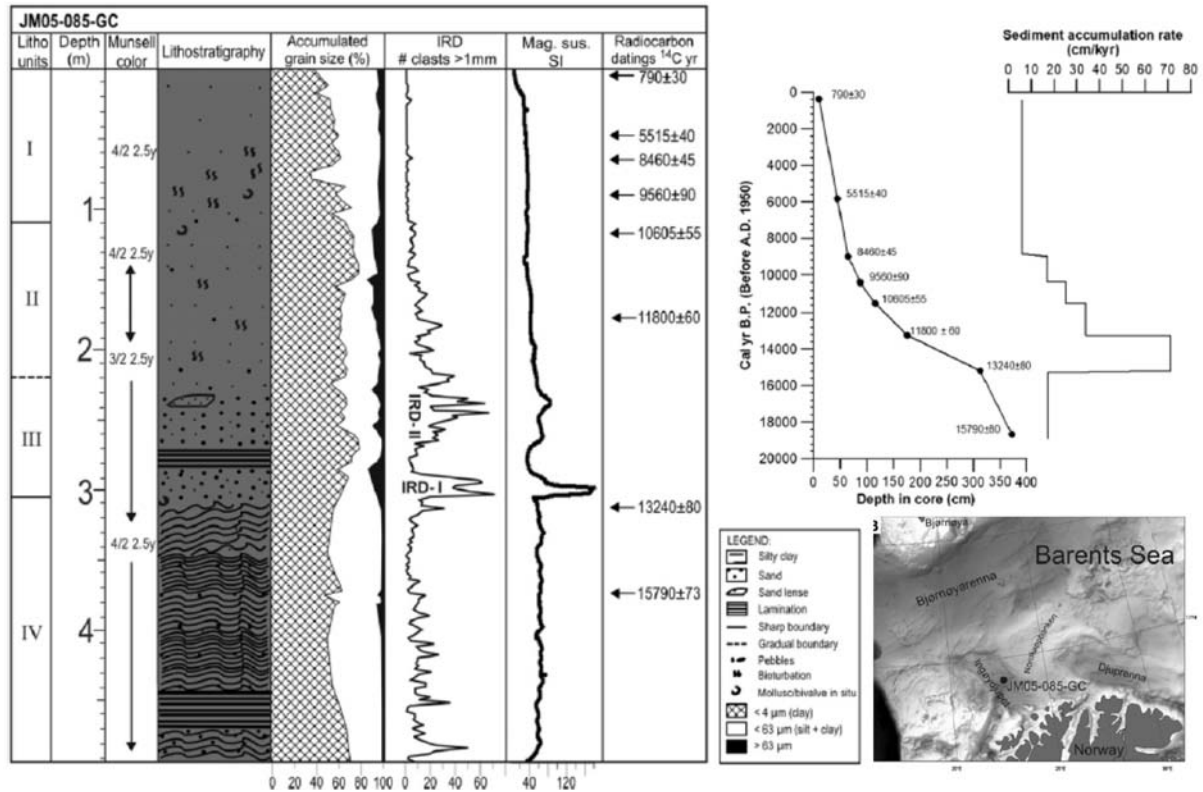


Figure 15. Details of the sedimentation history since the Last Glacial Maximum in Ingøydjupet from core JM05-08-GC (Aagard Sørensen et al., 2010). Notice the high sedimentation rates during the initial periods of deglaciation. During the last 9000 years there was only 54 cm of sediment deposition in the deepest part of the Ingøydjupet indicating even less sedimentation in our study area.

A second stage of fluid flow may be related to leakage along regional faults. Concentration of acoustic gas flares along the Ringvassøy Loppa Fault complex and subsurface indication of fluids accumulated along stratigraphic boundaries indicate a focused fluid flow system (Fig. 16). The fluid flow at present is hence concentrated along these open faults and driven by formation properties such as permeability.

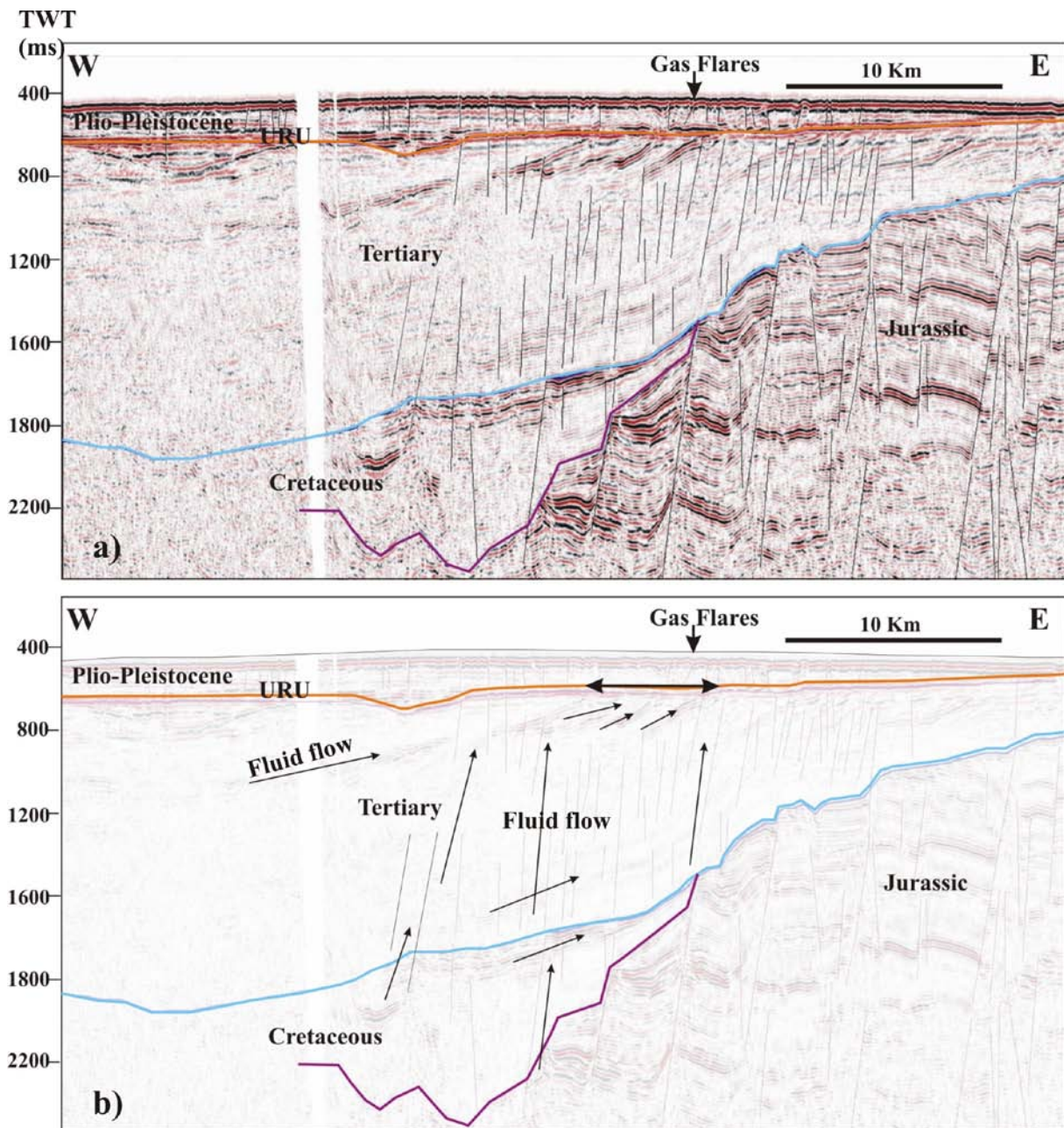


Figure 16. a) Seismic section and b) fluid flow model towards gas flares showing subsurface geology and fluid flow. The fluids are transported along intra-Tertiary permeable formations and the base of the Tertiary while highly fractured Tertiary and Cretaceous sediments allow fluid flow through open faults. Notice the large amount of fracturing in the Plio-Pleistocene allowing fluid flow through glacial till. See Fig. 13 for location.

5. CONCLUSIONS

1. Bathymetry and backscatter have given an overview of Holocene surface processes and their relation to subsurface geological processes. The backscatter data show typical signatures of pockmarks and iceberg ploughmarks. Numerous pockmarks were identified in the two basins along the study area. The pockmarks in most cases show high backscatter at their centres indicating sandy sediments or carbonates while large depressions observed scattered along the study area could be past events of explosive pockmark formation or simply prodmarks formed by plunging icebergs during the deglaciation.
2. Acoustic gas flares were identified close to regional fault complexes indicating active fluid flow, but with a different mechanism than gas hydrate melting.
3. Numerous fault like linear features aligned in NE-SW direction are observed on the seafloor along the eastern part of the study area. Detailed analysis of these using high resolution seismic data indicate that they could be reverse faults and/or till deposited at the reverse faulted boundaries.
4. The faults are inferred to be inactive since undisturbed, soft marine sediments with small pockmarks and iceberg plough marks can be observed above them but without direct spatial relationship to them.
5. Comparison of sedimentation rates from a dated core in the deepest part of Ingøydjupet and the high resolution seismic data indicate that the pockmarks formed after the deposition of glaciomarine sediments.
6. Pockmarks formed due to gas hydrate and the delay in their formation can be related to the slow processes of pressure and temperature transfer to the subsurface after deglaciation.

6. REFERENCES

- Aagaard-Sørensen, S., Husum, K., Hald, M., Knies, J., 2010. Paleooceanographic development in the SW Barents Sea during the Late Weichselian-Early Holocene transition. *Quaternary Science Reviews* 29, 3442-3456.
- Andreassen, K. & Hansen, T. 1995: Inferred gas hydrates offshore Norway and Svalbard. *Norsk Geologisk Tidsskrift* 45, 10-34.
- Bugge, T., Elvebakk, G., Fanavoll, S., Mangerud, G., Smelror, M., Weiss, H.M., Gjelberg, J., Kristensen, S.E., Nilsen, K., 2002. Shallow stratigraphic drilling applied in hydrocarbon exploration of the Nordkapp Basin, Barents Sea. *Mar. Pet. Geol.* 19, 13–37.
- Chand, S. & Minshull, T. A. 2003: Seismic constraints on the effects of gas hydrate on sediment physical properties and fluid flow: A review. *Geofluids* 3, 275-289.
- Chand, S., Mienert, J., Andreassen, K., Knies, J., Plassen, L., & Fotland, B. 2008: Gas hydrate stability zone modeling in areas of salt tectonics and pockmarks of the Barents Sea suggest an active hydrocarbon venting system. *Marine and Petroleum Geology* 25, 625-636.
- Chand, S., Thorsnes, T., Rise, L., & Bøe, R. 2009. Shallow Geology and seabed processes, Western Barents Sea, NGU Report 2009.041, pp 71.
- Eldholm, O., Sundover, E., Myhre, A.M. & Faleide, J.I. 1984: Cenozoic evolution of the continental margin off Norway and western Svalbard. In: AM Spencer (ed) *Petroleum geology of the North European Margin*, Graham and Trotman, London, 3-18.
- Eidvin, T. & Riis, F. 1989: Nye dateringer av de tre vestligste borehullene I Barentshavet. Resultater og konsekvenser for den tertiære hevingen. *NPD Contribution* 27, 44 pp.
- Eidvin, T., Brekke, H., Riis, F. & Rensaw, D.K. 1998: Cenozoic stratigraphy of the Norwegian Sea continental shelf 64°N – 68°N. *Norsk Geologisk Tidsskrift* 78, 125-151.
- Eidvin, T., Jansen, E. & Riis, F. 1993: Chronology of Tertiary fan deposits off the western Barents Sea: implications for the uplift and erosion history of the Barents Shelf. *Marine Geology* 112, 109-131.

Faleide, J.I., Solheim, A., Fiedler, A., Hjelstuen, B.O., Andersen, E.S., Vanneste, K. 1996: Late Cenozoic evolution of the western Barents Sea – Svalbard continental margin. *Global and Planetary change* 12, 53-74.

Hald, M., Sættem, J. & Nesse, E. 1990: Middle and Late Weichselian stratigraphy in shallow drillings from the southwestern Barents Sea: foraminiferal, amino acid and radiocarbon evidence. *Norsk Geologisk Tidsskrift* 70, 241-257.

Knies, J., Matthiessen, J., Vogt, C., Laberg, J.S., Hjelstuen, B.O., Smelror, M., Larsen, E., Andreassen, K., Eidvin, T. & Vorren, T.O. 2009: The Plio-Pleistocene glaciation of the Barents Sea-Svalbard region: a new model based on revised chronostratigraphy. *Quaternary Science Reviews* 28, 812-829.

Laberg, J. S., Andreassen, K., Knies, J., Vorren, T.O., Winsborrow, M., 2011. Late Pliocene-Pleistocene development of the Barents Sea Ice Sheet, *Geology*, 38, 107-110.

Lastochkin, A.N. 1977: Submarine valleys on the northern continental shelf of Europe, *Izv. Vsesoy. Geogr. Obsh.* 5, 412-417.

Long, D., Lammers, S., Linke, P., 1998. Possible hydrate mounds within large seafloor craters in the Barents sea. In: Henriot, J.P., Mienert, J., (eds.) *Gas Hydrates: Relevance to World Margin Stability and Climate Change*, vol. 137. Geological Society London Special Publication, 223–237.

Løseth, H., Lippard, S.J., Sættem, J., Fanavoll, S., Fjerdingsstad, V., Leith, L.T., Ritter, U., Smelror, M. & Sylta, O. 1992: Cenozoic uplift and erosion of the Barents Sea – evidence from the Svalis Dome area. In: TO Vorren et al (eds) *Arctic Geology and Petroleum Potential* (Norw. Pet. Soc. Spec Pub. 2, Elsevier Amsterdam, 639-661.

Mørk, M.B. & Duncan, R.A. 1993: Late Pliocene basaltic volcanism on the western Barents shelf margin: implications from petrology and $^{40}\text{Ar} - ^{39}\text{Ar}$ dating of volcani-clastic debris from a shallow drill core. *Norsk geologisk Tidsskrift* 73, 209-225.

Nansen, F. 1904: The bathymetrical features of the North Polar seas with a discussion of the continental shelves and previous oscillations of the shoreline. *Norwegian Polar Expeditions 1893-1896, Scientific results*, vol. IV, 231pp.

Norwegian Petroleum Directorate, 2005. NPD well report 7021/4-1, http://factpages.npd.no/ReportServer?/FactPages/PageView/wellbore_exploration&rs:Command=Render&rc:Toolbar=false&rc:Parameters=f&NpdId=135&IpAddress=193.156.2.1&CultureCode=nb-no

Nyland, B., Jensen, L.N., Skagen, J., Skarpnes, O. & Vorren, T. O. 1992: Tertiary uplift and erosion in the Barents Sea: Magnitude, timing and consequences. In: RM Larsen and H Brekke, TB Larsen and E Talleraas (eds), Structural and tectonic modeling and its application to petroleum geology, Norw. Pet. Soc. Spec. Publ. 1, Elsevier, Amsterdam, 153-162.

Nøttvedt, A., Berglund, T., Rasmussen, E. & Steel, R. 1988: Some aspects of Tertiary tectonics and sediments along the western Barents shelf. In: Morton AC, and Parson LM, (eds): Early Tertiary volcanism and the opening of the NE Atlantic. Geological Society of London, special publication 39, 421-425.

Riis, F. & Fjeldskaar, W. 1992: On the magnitude of the late Tertiary and Quaternary erosion and its significance for the uplift of Scandinavia and the Barents Sea. In: RM Larsen, H Brekke, BT Larsen, and E Talleraas (eds): Structural and tectonic modeling and its application to the Petroleum Geology NPF Special Publication 1, 163-185, Elsevier, Amsterdam.

Sheriff, R. 1980: Nomogram for Fresnel zone calculation. *Geophysics* 45, 968-972.

Shipley, T.H., Houston, M., Buffler, R.T., Shaub, F.J., McMillan, K.J., Ladd, J.W. & Worzel, J.L. 1979: Seismic reflection evidence for the wide spread occurrence of possible gas hydrate horizons on continental slopes and rises. *American Association of Petroleum Geologists* 63, 2204-2213.

Siegert, M.J., Dowdeswell, J.A., Hald, M., Svendsen, J.I., 2001. Modelling the Eurasian Ice Sheet through a full (Weichselian) glacial cycle. *Global and Planetary Change* 31, 367-385.

Sloan, E. D. 1990: *Clathrate Hydrates of Natural Gases*, Marcel Dekker, New York.

Solheim, A. & Elverhøi, A. 1985. A pockmark field in the central Barents Sea: gas from petrolgenic source ? *Polar Research*, 3, 11-19.

Solheim, A. & Kristoffersen, Y. 1984: Sediments above the upper regional unconformity: thickness, seismic stratigraphy and outline of the glacial history, *Norsk Polarinstitutt Skrifter* 179B, 26pp.

Spencer, A.M., Home, P.C. & Berglund, L.T. 1984: Tertiary structural development of western Barents shelf: Troms to Svalbard. In: AM Spencer (ed) *Petroleum geology of the North European Margin*, Graham and Trotman, London, 199-210.

Stoll, R.D. & Bryan, G.M. 1979: Physical properties of sediments containing gas hydrates. *Journal of Geophysical Research* 84, 645-648.

Sættem, J., Rise, L. & Westgard, D.A. 1992: Composition and properties of Glacigenic sediments in the southwestern Barents Sea. *Marine Geotechnology* 10, 229-255.

Vorren, T.O., Hald, M. & Lebesbye, E. 1988: Late Cenozoic environments in the Barents Sea. *Paleocenography* 3, 601-612.

Vorren, T.O., Kristoffersen, Y. & Andreassen, K. 1986: Geology of the inner shelf west of North Cape. *Norsk Geologisk Tidsskrift* 66, 99-105.

Vorren, T.O., Lebesbye, E., Andreassen, K. & Larsen, B. 1989: Glacigenic sediments on a passive continental margin as exemplified by the Barents Sea. *Marine Geology* 85, 251-272.

Vorren, T.O., Lebesbye, E. & Larsen, K.B. 1990: Geometry and genesis of the glacigenic sediments in the southern Barents Sea, In: Dowdeswell JA and Scourse JD, (eds) *Glacimarine environments, processes and sediments*, Geol Soc London, Sp Publ. 53, 309-328.

Vorren, T.O., Richardsen, G., Knutsen, S.M. & Henriksen, E. 1991: Cenozoic erosion and sedimentation in the western Barents Sea. *Marine and Petroleum Geology* 8, 317-340.

Winsborrow, M.C.M., Andreassen, K., Corner, G.D., Laberg, J.S., 2010. Deglaciation of a marine-based ice sheet: Late Weichselian palaeo-ice dynamics and retreat in the southern Barents Sea reconstructed from onshore and offshore glacial geomorphology. *Quaternary Science Reviews*, 29, 424-442-

WOD, 2005. World Ocean Database, (2005)
<http://www.nodc.noaa.gov/General/temperature.html>.



Norges geologiske undersøkelse
Postboks 6315, Sluppen
7491 Trondheim, Norge

Besøksadresse
Leiv Eirikssons vei 39, 7040 Trondheim

Telefon 73 90 40 00
Telefax 73 92 16 20
E-post ngu@ngu.no
Nettside www.ngu.no

*Geological Survey of Norway
PO Box 6315, Sluppen
7491 Trondheim, Norway*

*Visitor address
Leiv Eirikssons vei 39, 7040 Trondheim*

*Tel (+ 47) 73 90 40 00
Fax (+ 47) 73 92 16 20
E-mail ngu@ngu.no
Web www.ngu.no/en-gb/*